Sedimentology (1978) **25**, 307–338

Sand transport model of barchan dune equilibrium

A. D. HOWARD, J. B. MORTON,* MOHAMED GAD-EL-HAK† *and* DEBORAH B. PIERCE‡

*Department of Environmental Sciences and *Department of Engineering Systems and Science, University of Virginia, Charlottesville, Virginia* 22903, *†Flow Research Corporation, Seattle, Washington and ‡Westinghouse Nuclear Center, Monroesville, Pennsylvania*

ABSTRACT

Erosion and deposition over a barchan dune near the Salton Sea, California, is modelled by book-keeping the quantity of sand in saltation following streamlines of transport. Field observations of near-surface wind velocity and direction plus supplemental measurements of the velocity distribution over a scale model of the dune are combined as input to Bagnold-type sand-transport formulae corrected for slope effects. A unidirectional wind is assumed. The resulting patterns of erosion and deposition compare closely with those observed in the field and those predicted by the assumption of equilibrium (downwind translation of the dune without change in size or geometry). Discrepancies between the simulated results and the observed or predicted erosional patterns appear to be largely due to natural fluctuation in the wind direction. Although the model includes a provision for a lag in response of the transport rate to downwind changes in applied shear stress, the best results are obtained when no delay is assumed.

The shape of barchan dunes is a function of grain size, velocity, degree of saturation of the oncoming flow, and the variability in the direction of the oncoming wind. Smaller grain size or higher wind speed produce a steeper and more blunt stoss-side. Low saturation of the inter-dune sandflow produces open crescent-moon-shaped dunes, whereas high saturation produces a whaleback form with a small slip face. Dunes subject to winds of variable direction are blunter than those under unidirectional winds.

The size of barchans could be proportional to natural atmospheric scales, to the age of the dune, or to the upwind roughness. The upwind roughness can be controlled by fixed elements or by the sand is saltation. In the latter case, dune scale may be proportional to wind velocity and inversely proportional to grain size. However, because the effective velocity for transport increases with grain size, dune scale may increase with grain size as observed by Wilson (1972).

INTRODUCTION

The barchan appears to be the only stable transverse dune occurring in isolation on flat terrain with a partial sand cover. In fact, transverse dune complexes in areas of

0037–0746/78/0200–0307 $02.00

unidirectional wind generally appear to be coalesced barchanoid dunes. Barchans form under a regime of strong winds blowing from a nearly constant direction (Bagnold, 1941; Melton, 1940; Long & Sharp, 1964; McKee, 1966; Smith, 1970) and are remarkable in that they preserve their form and size while migrating long distances downwind (Long & Sharp, 1964; McKee, 1966; Hastenrath, 1967). Despite a voluminous descriptive literature and a few quantitative measurements of form, rate of migration, and sedimentary texture, a quantitative explanation of the geometry, size, and self-preserving nature of these transverse dunes has been lacking.

Because of its simple form (Fig. 1) and the ease of field measurements, the barchan dune affords an ideal starting point for examining the sedimentary processes causing transverse dunes in air and water. The approach reported here involves modelling of the sedimentary budget of a natural barchan. Observations of wind shear and direction of surface wind over the dune are coupled with sand-transport relationships of the Bagnold type which are corrected for the effects of surface slope on the quantity and mean direction of transport to predict the pattern of erosion and deposition on the dune. This pattern is compared with that implied by self-preservation of form during downwind translation. Although the numerical results apply to a particular dune at a particular time, the model can be applied to any dune given the wind field over the dune. Furthermore, the model illustrates the interactions of sand transport and the airflow that control the geometry and size of barchans.

In the model rates of erosion or deposition are predicted by following the changes in sediment transport capacity that occur along assumed streamlines of transport (Fig. 2). In moving a distance δx downwind both the distance between streamlines, l, and the sediment transport capacity, q (measured in mass of sand transported per unit of time per unit width), will in general change. Changes in sediment discharge occur because of changes in surface shear stress and because of change in inclination

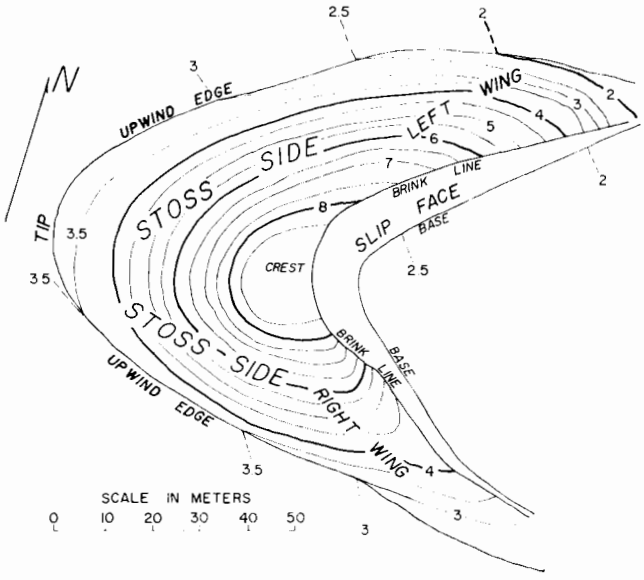

Fig. 1. Topographic map of the prototype barchan dune near the Salton Sea, California, with terminology. Note that 'stoss side' refers to the entire dune surface upwind of the flow separation at the brinkline.

and orientation of the slope relative to the oncoming wind. The rate of erosion over the interval δx is given by:

$$\frac{\delta h}{\delta t} = \frac{2(q_1 l_1 - q_2 l_2)}{\gamma(l_1 + l_2)\delta x} = -\frac{1}{\gamma}\left(\frac{q}{l}\frac{\delta l}{\delta x} + \frac{\delta q}{\delta x}\right), \tag{1}$$

where the second expression is the governing differential equation, the subscripts $_1$ and $_2$ refer to the positions at the upwind and downwind ends of the interval, δx, respectively, and γ is the bulk density of the sand. A similar equation was derived for largescale sandflow by Wilson (1971, p. 194). Erosion may therefore occur either by divergence of transport streamlines or from increase in sediment transport capacity in a downstream direction.

This study provides answers to many basic questions about dune processes, including the following:

(1) are Bagnold-type transport relationships adequate to predict sediment discharge on the sloping surfaces of a dune where flow velocities change rapidly downwind? (2) in view of the non-logarithmic velocity profiles over dunes, can measurements of wind velocity near the sand surface yield the shear stress felt by the sand in transport? (3) do downwind changes in the surface shear cause immediate changes in sand transport, or is there a time (distance) lag? (4) do changes in assumed grain size or wind velocity alter the simulated pattern or erosion and deposition? and (5) how will a barchan respond to a change in wind direction?

The following sections outline the simulation model, considering in turn (1) the spatial distribution of erosion and deposition consequent to the assumption of self-preservation, (2) the sand-transport equations, (3) the empirical data on dune geometry, wind velocity and direction, and erosion rates used to verify the model, (4) the structure of the simulation model, (5) the comparison of the simulated erosion and deposition rates with the pattern expected for self-preservation, and (6) the influence upon dune form and size of the factors of wind velocity, variability of wind direction, grain size, percentage saturation of the interdune sandflow, interdune aerodynamic roughness, and time.

EQUILIBRIUM OF BARCHANS

The Stoss side

In the following discussion a unidirectional wind is assumed; since natural dunes are subject to somewhat variable wind directions, the unidirectional wind is considered to be an appropriate vector average. Self-preservation of form (i.e. equilibrium) requires that the rate of translation in the direction of the oncoming wind, $\delta x/\delta t$, be constant on all parts of the dune, although it may vary temporally (the oncoming wind is defined as the direction of the undisturbed unidirectional wind, as compared to the topographically-deflected local wind near the surface of the dune). As Fig. 3A and B illustrates, the rate of change of surface elevation, $\delta h/\delta t$, for a given rate of translation is related to the slope angle, θ, and to the angle between the oncoming wind and the contour strike, η, by the following (Allen, 1968, pp. 100–101):

$$\frac{\delta h}{\delta t} = \frac{\delta x}{\delta t}\,\mathrm{Sin}\,\eta\,\mathrm{Tan}\,\theta \tag{2}$$

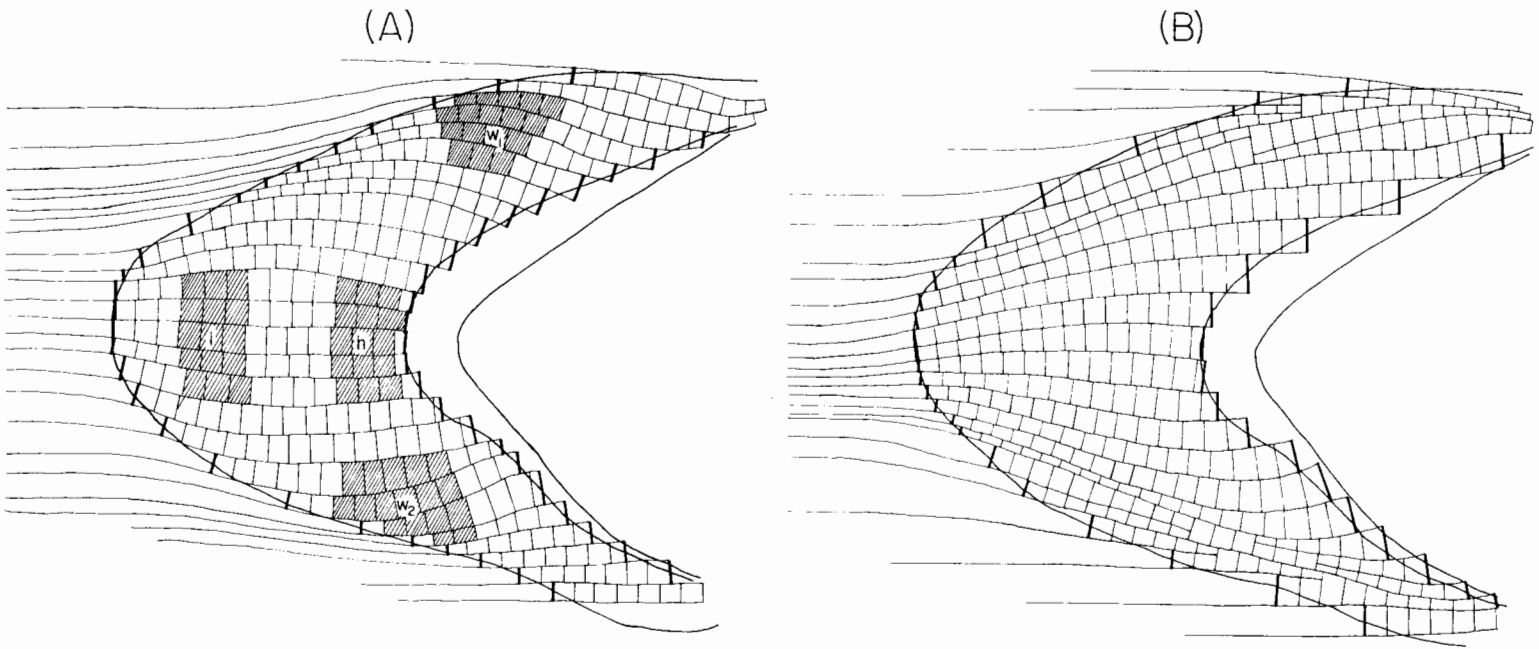

Fig. 2. Transport streamline maps, showing division of streamline lanes into cells. Heavy lines define upwind boundary of upwind edge cells and downwind end of brinkline cells: (A), Transport assumed to follow the near-surface wind. Shaded areas discussed in text; (B), Transport assumed to move perpendicular to ripple crests.

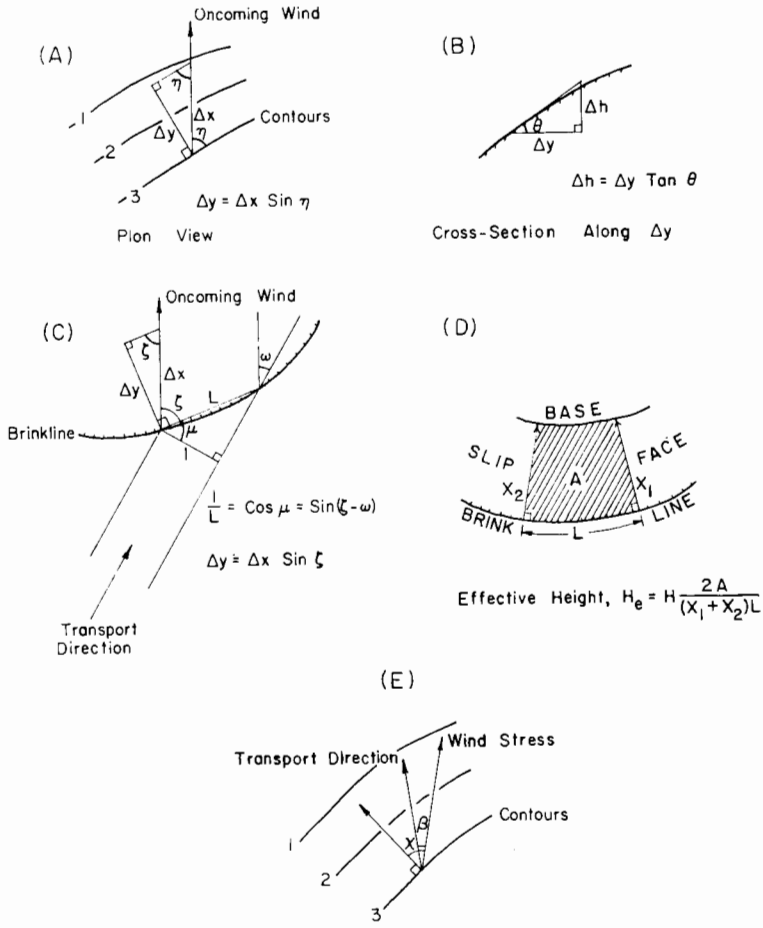

Fig. 3. Geometrical relationships and definitions. A and B, stoss side equilibrium; C and D, crestline equilibrium; E, deflection of transport direction from direction of applied stress.

The Leeside

The equilibrium of the lee, or slip face is likewise governed by Equation 2. However, on the higher portions of the slip face most of the saltation and creep load is deposited near the brink and is redeposited over the slip face by repeated avalanching. The assumption of avalanche redistribution allows the treatment of slipface equilibrium by specification of the equilibrium of the brinkline, which is generally a line of separation of the flow, dividing the normal downwind flow on the stoss side from reverse circulation on the lee face (Coursin, 1964; Allen, 1968; Howard, unpublished field observations). Analogously to the stoss side equilibrium, the consequence of self-preservation under a unidirectional wind is that the rate of translation of the brink in the direction of the wind is uniform at all points of the brinkline, and that the brink height is constant through time. Figure 3C shows that the volume rate of sediment delivery per unit length of brink is given by:

$$\frac{q}{\gamma} \text{Sin } (\zeta - \omega)$$

where ζ is the angle between the oncoming wind and the brinkline and ω is the angle between the oncoming wind and the transport direction. The volumetric rate of addition to the slip face per unit brink length is $H(\delta y/\delta t)$ where $\delta y/\delta t$ is the rate of movement of the brinkline perpendicular to the brink and H is the height of the brinkline above the toe of the dune. However, because of curvature, the brink height must be replaced by an 'effective height' H_e, as indicated in Fig. 3D. At equilibrium the above quantities are equal:

$$H_e \frac{\delta y}{\delta t} = H_e \frac{\delta x}{\delta t} \text{Sin } \zeta = \frac{q}{\gamma} \text{Sin } (\zeta - \omega),$$

or,

$$q = K\gamma \frac{H_e \text{Sin } \zeta}{\text{Sin } (\zeta - \omega)} \tag{3}$$

where $K = \delta x/\delta t$, a constant on all parts of the brinkline.

EQUATIONS OF SEDIMENT TRANSPORT

The relationships between the rate of sediment transport and the wind shear has been summarized in several sets of equations derived from extensive field and laboratory experiments. Because of the interaction between the saltating grains and the near-surface wind, the velocity distribution near the ground on a flat, naturally rippled sand surface is modified, when sand is in motion, from the usual logarithmic profile by the addition of a constant, U_t (Bagnold, 1941, p. 61; Zingg, 1953, p. 121):

$$v(z) = \frac{v_*}{\kappa} \ln \left(\frac{z}{k} \right) + U_t, \tag{4}$$

where κ is von Karman's constant, k is a reference height, U_t is the velocity at the threshold of motion at $z = k$, and v_* is the shear velocity. The apparent roughness height in saltation, z_{0a}, is not independent of the wind strength. Equation 4 plots linearly on semi-logarithmic paper, so that the profile for a given wind shear can also be described by:

$$v(z) = \frac{v_*}{\kappa} \ln\left(\frac{z}{z_{0a}}\right) \tag{5}$$

where

$$z_{0a} = k \exp(-\kappa U_t / v_*) \tag{6}$$

The best-known transport formula was developed by Bagnold (1941, p. 66):

$$q = C\left(\frac{d}{D}\right)^{\frac{1}{2}} \cdot \frac{\rho}{g} v_*^3 \tag{7}$$

where, ρ is the fluid density, d is the grain diameter and D is the reference grain diameter (0·25 mm in Bagnold's experiments), and C is a constant with a value of about 1·8 for naturally graded sand. Thus estimation of sediment discharge requires determination of the shear velocity. This can be done by measurement of wind velocity at one or more heights above the sand surface, assuming equation 4 to be valid. This approach has been used in the present model.

Other empirical studies have summarized their results with transport formulae nearly identical to equation 7 (Zingg, 1953, p. 128; Williams, 1964, p. 280). Formulae of this form are unrealistic in that they predict a small transport rate for shear velocities below the threshold of motion. To remedy this, Lettau & Lettau (in press) have proposed a formula that includes the critical shear stress at the initiation of motion, v^*_t:

$$q = \begin{cases} C'\left(\frac{d}{D}\right)^{\frac{1}{2}} \cdot \frac{\rho}{g}(v_* - v_{*t}) v_*^2 & v_* > v_{*t} \\ 0 & v_* \leqslant v_{*t} \end{cases} \tag{8}$$

Transport rates predicted by this formula differ from the Bagnold equation only at wind velocities very close to the threshold of motion. A similar equation is implied in later theoretical work by Bagnold (1956, p. 294):

$$q = \begin{cases} C''\left(\frac{d}{D}\right)^{\frac{1}{2}} \cdot \frac{\rho}{g}(v_* - v_{*t})^2 v_* & v_* > v_{*t} \\ 0 & v_* \leqslant v_{*t} \end{cases} \tag{9}$$

The shear velocity at the threshold of motion is a function of the grain size, the sediment density, σ, and the dynamic friction angle, α, which is a characteristic of the sediment shape and surface packing. Bagnold's formula for this relationship (1941, p. 86) is adequate for dune sands (Howard, 1977), although more complicated formulae taking into account lift and interparticle attraction have been proposed (Chepil & Woodruff, 1963, pp. 222–229; Iverson *et al.*, 1976):

$$v_{*t} = F(\text{Tan}\,\alpha \cdot d)^{\frac{1}{2}}, \text{ where } F = B\left[\frac{(\sigma - \rho)g}{\rho}\right]^{\frac{1}{2}} \tag{10}$$

and B is a dimensionless constant. The threshold velocity and reference height in equation 4 may also be functions of grain size. Bagnold (1941, p. 105) suggests that this reference height is independent of grain size, but that the threshold velocity is not:

$$U_t = \frac{F}{\kappa} \cdot (\text{Tan}\,\alpha \cdot d)^{\frac{1}{2}} \cdot \ln\left(\frac{30}{d}\right)$$

Zingg (1953, p. 121) finds that both k and U_t depend upon grain size: $k = 10\,d$; $U_t = 8950\,d$ (cgs units). For the simulations reported below k was assumed to be constant, but U_t was allowed to vary with grain size at a rate intermediate between the results of Bagnold and Zingg:

$$U_t = E \cdot \frac{F}{\kappa} \cdot (\text{Tan}\,\alpha \cdot d)^{\frac{1}{2}} \tag{11}$$

where E is a constant.

Sand transport on dunes is affected by the slope of the surface, being inhibited on the windward slopes and enhanced by a downslope gradient. Unfortunately, no systematic experimental data has been collected for transport on inclined surfaces, so that equations 7–9 must be corrected for slope by available theory. Slope effects enter directly into the transport equation (equations 7–9) as a result of the effects of slope on the motion of saltating grains, and indirectly by the effects of slope on the threshold of motion (equations 10–11). Existing theory and observation seems adequate to account for the effects of slope on threshold velocity, U_t, threshold shear, v_{*t} and reference height, k. The threshold shear on a sloping surface can be calculated by replacing Tan α in equation 10 by a more complicated function of α, the slope angle, θ, and the angle between the local wind and the direction of the normal of the slope (Howard, 1977):

$$v^2_{*t} = F^2 \cdot d \cdot [(\text{Tan}^2\,\alpha\,\text{Cos}^2\,\theta - \text{Sin}^2\,\chi\,\text{Sin}^2\,\theta)^{\frac{1}{2}} - \text{Cos}\,\chi\,\text{Sin}\,\theta] \tag{12}$$

The threshold velocity, U_t, can be similarly corrected:

$$U_t = E \cdot \frac{F}{\kappa} \cdot d^{\frac{1}{2}} \cdot [(\text{Tan}^2\,\alpha\,\text{Cos}^2\,\theta - \text{Sin}^2\,\chi\,\text{Sin}^2\,\theta)^{\frac{1}{2}} - \text{Cos}\,\chi\,\text{Sin}\,\theta]^{\frac{1}{2}} \tag{13}$$

The reference height, k, is assumed to be constant.

The direct effects of slope on transport are less certain. From considerations of the general force and energy balance, Bagnold (1956, p. 294; 1973, p. 482) has suggested that the transport on a sloping surface can be expressed as:

$$q' = \frac{q}{\text{Cos}\,\theta'\,(\text{Tan}\,\alpha + \text{Tan}\,\theta')} \tag{14}$$

where q' is the sediment transport rate on the sloping surface, q is the equivalent rate on a flat surface (from equations 7–9), and θ' is the slope of the surface in the direction of transport ($\text{Tan}\,\theta' = \text{Tan}\,\theta\,\text{Cos}\,\chi$). Because of the lack of empirical verification of equation 14, the degree of sensitivity of the pattern of erosion and deposition predicted by the composite model was tested by simulations employing both the correction for slope effect (equation 14) and the uncorrected formulae (equations 7–9).

DATA

Observations on a representative barchan dune in the Salton Sea dune field during a two-week period in June 1973, provided the data on dune geometry, sand transport, and wind flow that were used to construct and verify the simulation model. The observations were supplemented by detailed laboratory measurements of the distribution of wind velocities over a scale model of the dune. The procedures of the measurements and the assumptions in the analysis are discussed in Howard *et al.* (1977). A summary is presented below. The field data utilized in the simulation model consisted of the following.

(1) A plane table survey (Fig. 1) provided the data on slope gradient and orientation and on brinkline geometry.

(2) Observations of near-surface wind directions and ripple mark orientations and sixty-three locations on the dune were made during or after three sand-blowing winds. The wind direction observations were used to make a map of streamlines of near-surface airflow for a wind from S82°W (Fig. 2A), which was inferred to be the dominant direction of sand transport from aerial photographic measurement of the orientation on the dark, sand-free tails extending from the centre of the barchans. Although the movement of saltating grains nearly parallels the near-surface wind, the coarser creep load, which is impelled along the surface by wind stress and saltation impacts, is deflected downslope from the direction of the wind in proportion to the surface gradient (Howard, 1977). The magnitude of the deflection of the creep motion from the direction of the wind stress (Fig. 3E) is (Howard, 1977):

$$\text{Sin}\,\beta = \frac{\text{Tan}\,\theta\,\text{Sin}\,\chi}{\text{Tan}\,\alpha} \tag{15}$$

Ripple crests are perpendicular to the movement of the creep load and thus are similarly deflected. Data from ripple mark crests were used to construct a streamline map for the creep load for a wind from S82°W (Fig. 2B). Because the direction of

mean transport lies between the surface wind and the perpendiculars to the ripple crests, simulations of sand transport were conducted with both sets of streamlines.

(3) The simulations assume that the grain size of the sand in motion was constant over the dune, because the sand arriving from upwind is likely to be laterally uniform in size and little variation in grain size occurs along the slip face, where most of the sand accumulates.

(4) Changes in surface elevation and rate of advance of the brinkline were measured during the two-week period of field observations. This empirical data on erosion and deposition rates (Fig. 4A) can be compared with the theoretical rates implied by self-preservation (equation 2 and Fig. 4B). The empirical rates are close to the theoretical distribution; the empirical rates were fit by linear regression to an equation of the form of equation 2:

$$\Delta h = 1{\cdot}59 \operatorname{Sin} \gamma_i \operatorname{Tan} \theta \; (n = 63; r = 0{\cdot}87) \tag{16}$$

where Δh are the observed elevation changes, γ_i and θ were estimated from the contour map of the dune, and the fitted constant gives the estimated downwind translation of the dune, in metres (which is close to the observed movement of the brinkline).

(5) Near-surface wind speeds at heights of 69 and 230 cm above the surface were measured at thirteen locations on the stoss side and brink (Fig. 5). During the period of measurements the oncoming winds varied through a directional range of 30 degrees. However, all but two measurements were made within a 15 degree range.

Because of the paucity of field measurements of velocities, profiles of wind speed were measured over a number of points on a model dune in a wind tunnel simulating the atmospheric boundary layer. Details of the scaling procedures are discussed in Howard *et al.* (1977). The lowest measurements over the model were taken at a height of 0·25 cm, which with the geometric scale factor of 315 is equivalent to a height of 80 cm above the prototype dune surface. The laboratory measurements were scaled slightly for an unbiased fit to the field measurements (Fig. 6). The remaining scatter between field and laboratory measurements is largely due to variation in the wind direction during field measurements.

THE SIMULATION MODEL

Erosion and deposition on stoss-side

The stoss side simulation entails the estimation of erosion or deposition rates at intervals of approximately 3 m (prototype scale) along the assumed paths of sediment transport from the leading edge to the brink (Fig. 2). The streamlines are broken into cells and erosion and deposition within each cell is calculated using equation 1, which requires estimates of the sediment discharge, q, entering and leaving the cell and of the divergence of the sediment flow, $(q/l)\cdot(\delta l/\delta x)$. The flow divergence, $\delta l/\delta x$, can be measured by the widths of the upstream and downstream ends of the cell (l_1 and l_2, respectively, so that:

$$\frac{\delta l}{\delta x} = \frac{l_2 - l_1}{x} \tag{17}$$

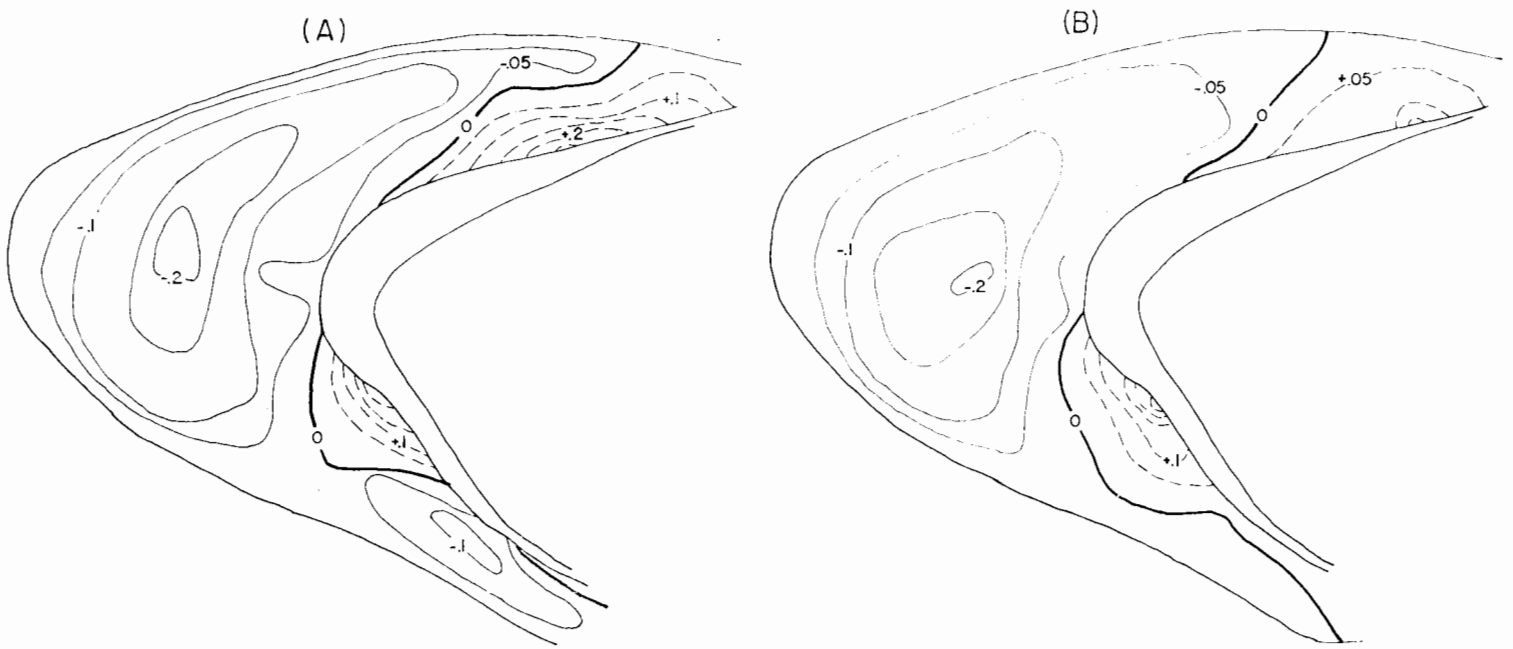

Fig. 4. Scaled erosion and deposition rates on prototype barchan. Solid contours indicate erosion, dashed show deposition: A, rates observed during 2-week period in field on prototype barchan: B, rates predicted by assumption of translation without change of size or shape in direction of dominant wind.

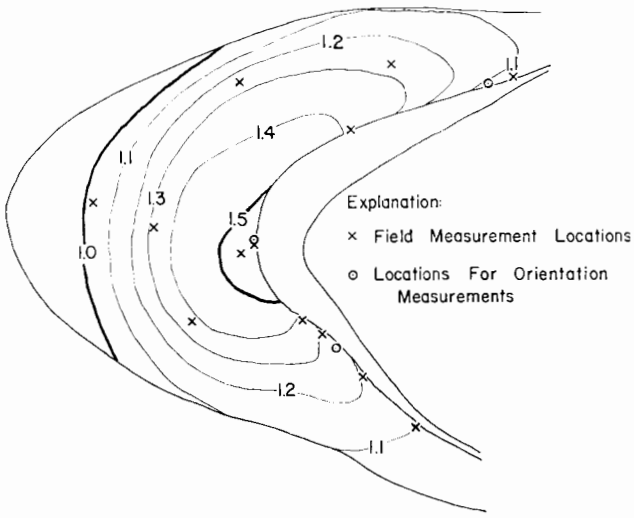

Fig. 5. Contours of velocity measured over model dune. Contours show value of $v(80)/v_0$ (80).

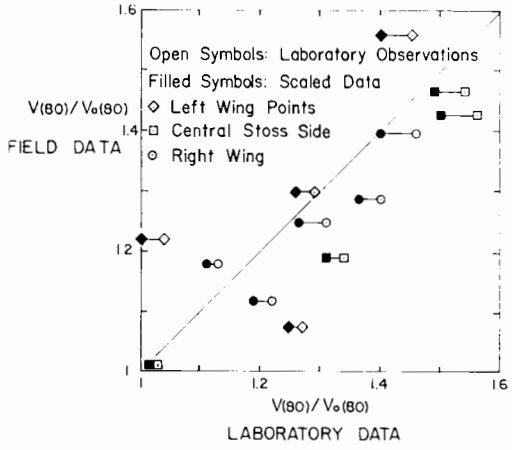

Fig. 6. Relationships between velocities measured in field and over model dune at equivalent heights. Filled symbols show scaling of laboratory data to eliminate bias.

where x is the cell length in the direction of the wind. However, for the small values of divergence over the dune, a more accurate estimate results from the use of a contour map of the angular deviation of the surface wind from the oncoming wind, where the angle of deviation was read for the four corners of each cell, the divergence being given by:

$$\frac{\delta l}{\delta x} = \frac{\psi_{ur} + \psi_{dr} - \psi_{ul} - \psi_{dl}}{2} \tag{18}$$

where the local wind deviation, ψ, is measured in radians and the subscripts refer to upstream, u, downstream, d, left, l, and right, r (viewing downstream).

The local transport rate, q, was estimated at the upstream and downstream ends of each cell, which requires the specification of several parameters. The angular relationships, θ, ψ and χ varied over the dune and were evaluated for each cell end by the use of contour maps of these quantities. The constants B, D, E, and C (or C' or C''), as well as the sediment and fluid density, σ and ρ, and the dynamic friction angle, α, were given fixed values (Table 1). The grain size, d, was specified as an input variable, and was usually assumed to be constant over the dune. The shear velocity, v_*, was specified by the field and wind tunnel measurements of near-surface velocities over the dune and scaled by an assumed undisturbed upwind velocity $v_0'(z)$. The wind velocities measured in the laboratory at 0·25 and 0·5 cm above the dune surface (80 and 160 cm, prototype scale) were scaled with respect to the oncoming wind at the same level, $v_0(z)$, and contour maps of $V(z) = v(z)/v_0(z)$ were prepared for the two heights (Fig. 5).

Table 1. Values of fixed parameters

Parameter	Value
B	0·13
C	1·8
C'	4·2
C''	5·0
E	6·4
k (cm)	0·3
D (cm)	0·025
g (cm²/sec)	980
ρ (g/cm³)	0·0012
σ (g/cm³)	2·65
α (degrees)	30·5

The shear velocity, v_*, was calculated from the contour maps, assuming that the shear velocity is constant below the lowest level of measurement (80 cm, prototype scale), so that equation 4 can be used to calculate v_*:

$$v_* = \frac{\kappa(V(80) \cdot v_0'(80) - U_t)}{\ln(80/k)} \tag{19}$$

where $v_0'(80)$ and k are input parameters for the simulations, and U_t was calculated from equation 13 for the assumed grain size. Simulations of two-dimensional turbulent flow by Taylor & Gent (1974) indicate that the shear velocity is nearly constant to about the relative level, z/H, of the present measurements. Profiles of velocity at the brink of the dune compare closely with these simulations, and suggest a nearly constant shear stress below the 80 cm level of measurement (prototype scale) (Fig. 7).

If the sand discharge at a given point is in equilibrium with the shear velocity at that same point, equations 7–9 can be used directly to estimate the discharge at the upstream and downstream ends of each cell. However, some researchers feel that changes in sediment transport lag behind changes in shear stress and that this lag

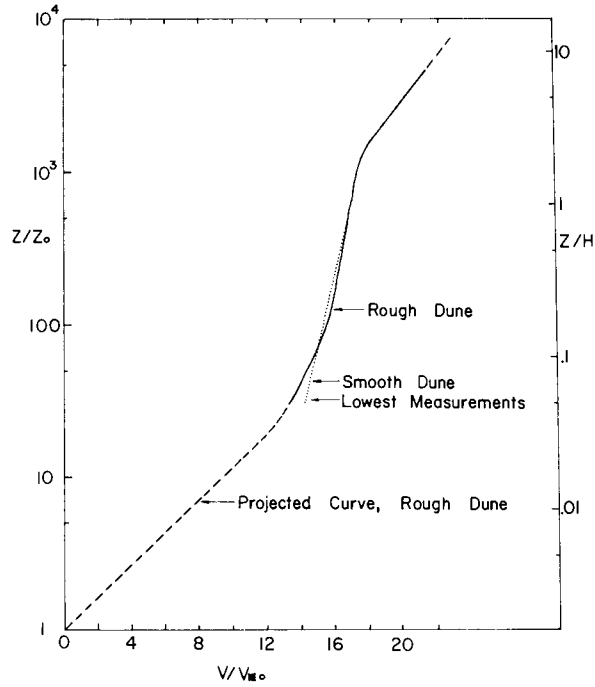

Fig. 7. Velocity profile over centre of brinkline, showing acceleration of near-surface flow. Based on laboratory measurements over rough and hydraulically smooth model dunes.

might, in fact, cause the unstable relationship between sand transport and near-surface wind responsible for the formation of dunes (Bagnold, 1956, p. 294; Kennedy, 1969, p. 154; Reynolds, 1965), whereas Raudkivi (1966) feels no lag is necessary. To test these hypotheses, the actual transport rate at a point, q_a, was assumed to be a weighted function of the equilibrium transport rate at that point, q_e, and of the actual transport rate at upwind points. A geometric weighting of upwind actual discharges was adopted:

$$q_{at} = \frac{q_{e1}}{\lambda+1} + \sum_{i=2}^{n} \frac{q_{ai}}{\lambda+1} \cdot \left(\frac{\lambda}{\lambda+1}\right)^{i-1} \tag{20}$$

where the subscript i refers to successive upwind streamline cell boundaries to the current cell boundary at $i = 1$. The parameter λ is the average delay length in units of cells; a delay of zero is equivalent to a transport rate in equilibrium with the shear stress. The number of upwind transport rates, n, taken into account was eleven for average delays less than three cells (about 9 m) and twenty-six for delays up to ten cells. The weights were adjusted for the finite series of equation 20 so as to sum to unity. The geometric distribution is a discrete approximation to the exponential, and appears to provide a realistic modelling of a lag in transport rate.

The discharge upwind of the first cell on the dune at the upwind edge is assumed to be uniform and equal to the equilibrium transport rate over a sand surface times

an assumed percentage saturation, P, for the upwind flow. Since the sand upwind from a barchan is generally transported over a desert pavement or other immobile surface it may be unsaturated relative to a loose sand surface. In fact, due to the high rebound of sand grains on a hard surface (Bagnold, 1941, p. 7; Ellwood, Evans and Wilson, 1975), Bagnold (1941) suggests that the flow could be oversaturated relative to a loose sand surface. Thus the actual transport rate at any point on the dune is a function of both λ and P, and both are specified as input to the simulations. However, if equilibrium transport is assumed ($\lambda = 0$), the degree of upwind saturation affects the rates of erosion and deposition only at the first cell of each streamline lane at the upwind edge.

Slip-face migration

The simulated rate of translation of the slip face in the direction of the oncoming wind is a function of the sediment discharge at the brink, of the effective slip face height, and of the geometrical relationships at the brink (equation 3). This rate was evaluated at each streamline terminating at the brinkline (Fig. 2).

RESULTS

The product of the simulation model is the distribution of predicted rates of erosion and deposition over the stoss-side and rates of translation of the slip face in the direction of the oncoming wind. These results are to be compared with the theoretical erosion and deposition rates predicted by the criterion of self-preservation or with the empirical rates observed during the field study. To effect this comparison, the simulated, theoretical, and empirical rates must be normalized by division by the rate of downwind translation of the dune, so that erosion or deposition is expressed per unit downwind translation of the dune, that is, by $\delta h/\delta x$. Normalized theoretical erosion rates are given by dividing both sides of equation 2 by the translation rate, $\delta x/\delta t$ (Fig. 4B). The empirical rates are normalized by the estimated regression slope of equation 16 (Fig. 4A). The simulated rates can be normalized either by (1) the median of the translation rates estimated at the brinkline terminations of the individual streamline lanes, or (2) by the average value of the translation rates estimated for each cell by use of equation 2. The former method was used because it does not presuppose the validity of equation 2 and because it ties together the brinkline and stoss-side equilibria.

Stoss side

As with most models of physical processes, this sediment budget model will be considered a success to the degree that the simulated patterns of surface changes over the dune agree with either the empirical or theoretical patterns. The degree of this agreement is assessed by several quantitative measures. The average difference between the simulated erosion and deposition rates and the empirical (or, alternatively, the theoretical) rates for each streamline cell on the stoss side is termed the bias:

$$b = \frac{\sum_{i=1}^{n} (s_i - o_i)}{n} \tag{21}$$

where b is the estimated bias, s_i is the simulated rate of change, o_i is the empirical (or theoretical) rate, and n is the number of streamline cells. The degree of variation is measured by the variance of the differences between the simulated and empirical rates, corrected for the bias:

$$v = \frac{\sum_{i=1}^{n} (s_i - o_i - b)^2}{(n-1)}. \tag{22}$$

Finally, the simulations are compared with expected results through the use of the standard correlation coefficient between s_i and o_i. Of these measures, the bias and variance are affected by the normalization of the simulated erosion rates by the translation of the brink. A low bias and variance will result only if the simulation model (1) reproduces the relative rates of erosion and deposition over the stoss side, and (2) simulates a rate of advance of the brink consistent with the erosion rates on the stoss side. The correlation coefficient measures only the first of these.

For comparison purposes the bias, variance, and correlation were calculated separately for the initial cells of the streamlines (the upwind edge) and for the remaining stoss side points (the core). This separation was made because the assumed initial undersaturation of the oncoming flow affects only the upwind edge cells for those simulations with no assumed lag. Also, the upwind edge cells were expected to show the greatest discrepancy between simulated and predicted erosion rates because the streamlines were poorly defined upstream of the upwind edge.

These comparative statistics were used to test the effects of variations in the parameters of the simulation model as well as the effects of more fundamental changes in the mathematical structure of the model. A nominal set of model parameters was assumed to which individual model variations could be compared. These represent a grain size (0·25 mm) and an undisturbed upwind velocity ($v_0'(80) = 1000$ cm/sec) that approximate the conditions on the prototype barchan, and a combination of transport law (Equation 9), delay ($\lambda = 0$), transport path (following the wind streamlines) and slope effect (equation 14) that is both physically reasonable and closely simulates the theoretical erosion and deposition rates. The major results of the simulations presented below are summarized from Howard *et al.* (1977).

(1) *Variation in velocity and grain size.* When the sand is assumed to follow the wind streamlines, the bias and variance of core cells show a weak dependence upon wind velocity and grain size (Fig. 8). For transport assumed to follow the ripple train, the bias, but not the variance, becomes a strong function of wind speed and grain size.

(2) *Lag of transport rate behind change of shear stress.* The effect of delays up to ten cells (about 32 m, prototype scale) were investigated for an assumed initial saturation of 50% (Fig. 9). The bias of core points is not markedly affected by increased

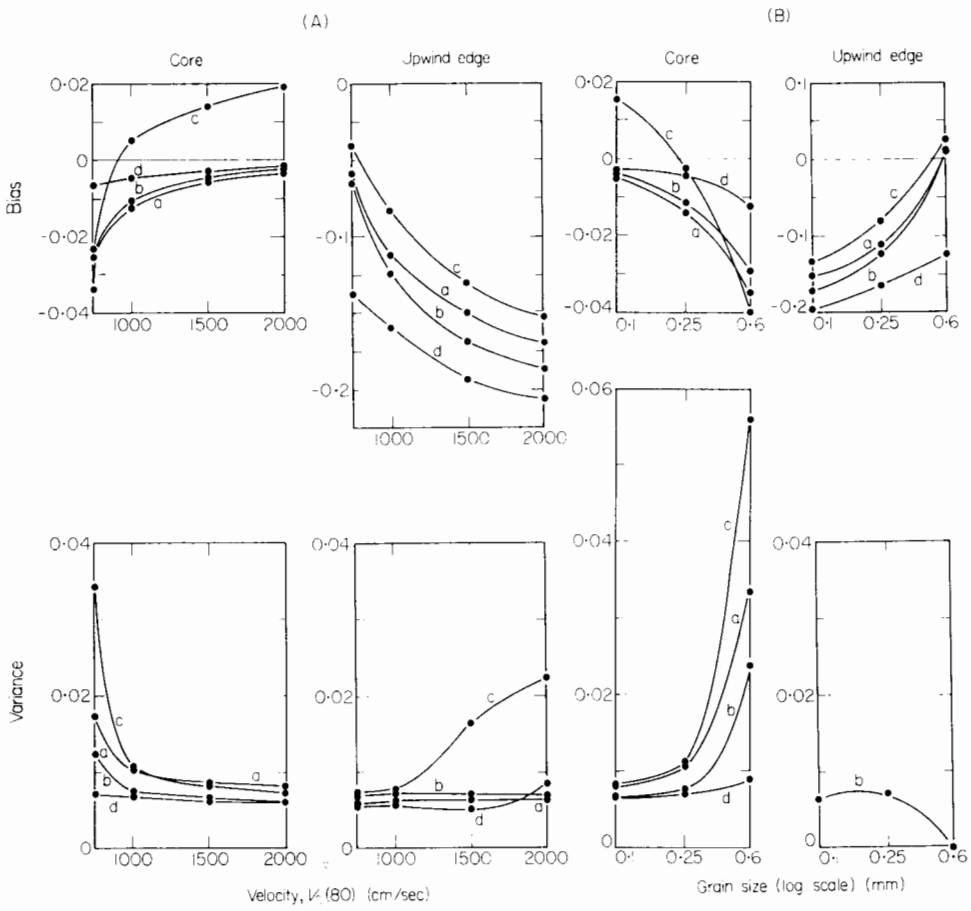

Fig. 8. Effect of velocity (A) and grain size (B) upon the bias and variance of simulated erosion and deposition rates for core (285 cells, wind streamlines and 326 cells, ripple streamlines) and leading edge cells (twenty-six cells, wind streamlines and twenty-four cells, ripple streamlines). a, Modified Bagnold formula, wind streamlines, slope effect retained; b, mod. Bag., wind, slope discounted; c, mod. Bag., ripple, slope discounted; d, original Bagnold, wind, slope discounted.

delay, whereas the bias of upwind edge cells decreases in absolute value as the delay increases from nil to about two cells. Variance of both core and upwind edge cells declines abruptly for short delays, then increases slowly for further delay. The decrease of core variance for short delays is due to the averaging effect of the delay function (equation 20), because similar, but even more marked reductions are effected by contouring the simulated erosion and deposition rates by hand (Fig. 10), which smooths out the local variance (Table 2). Neglecting the averaging effect, longer delays thus increase the variance.

(3) *Percentage saturation.* The percentage saturation required for equilibrium may be estimated by that value that results in zero average bias for the upwind edge cells. An initial saturation of about 80–85% is suggested (Fig. 9). A second approach estimates the amount of sand lost from the wingtips of the dune, but uncertainties in the sand budgeting make this estimate unreliable (Howard *et al.*, 1977).

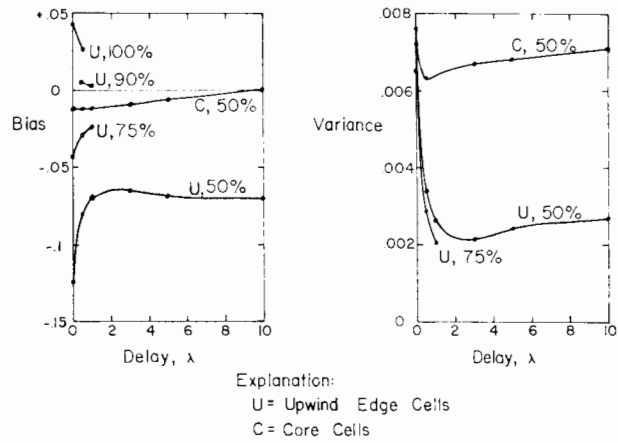

Fig. 9. Effect of delay and percent saturation upon bias and variance, for otherwise nominal conditions.

(4) *Slope effect.* Simulations were calculated using both the slope-corrected transport formulae (equation 14) and non-corrected formulae (equations 7–9). Simulations ignoring the slope effect resulted in lower absolute values of the bias and lesser variance than the slope-corrected formulae (Fig. 8).

(5) *Transport formula.* Simulations were made for the original and modified Bagnold formulae (equations 7 and 9) and the similar Lettau formula (equation 8). The three formulae produced very similar results for high velocities and/or small grain size, but whereas the original Bagnold formula produced bias and variance nearly independent of grain size and wind velocity, the other formulae produced sharply increased variances and greater negative bias for large grain size and low wind velocity, that is, near the threshold of motion.

(6) *Effect of divergence.* Discarding the divergence effects in equation 1 resulted in little change (Table 2). Variation in surface shear is thus more important in determining stoss side equilibrium than are the direct effects of sediment convergence and divergence.

(7) *Comparison with theoretical and empirical erosion rates.* The previous stoss side simulations were compared with the theoretical predictions. However, the hand-smoothed results (Fig. 10) were compared with both theoretical and empirical erosion rates (Table 2). The simulated rates agree nearly equally with the empirical and the theoretical rates with the exception of the bias, which is closer to zero for the theoretical rates.

(8) *Brinkline equilibrium.* The simulations are also judged by the degree to which they predict brinkline equilibrium. Values of sand discharge at the brink terminations of streamline lanes were plotted versus the factor

$$f = \frac{H_e \operatorname{Sin} \zeta}{\operatorname{Sin} (\zeta - \omega)}.$$

If the simulations predict a perfect equilibrium, the points plot on a straight line

Table 2. Comparison of simulated stoss-side erosion and deposition rates with observed and predicted rates

Transport‡ path	Slope§ effect	Delay (λ)	Convergence**	Correlation coefficients with†		Bias with†		Variance with†	
				Observed*	Predicted	Observed	Predicted	Observed	Predicted
W	*S*	0	*C*	0·56	0·59	−0·013	0·0002	0·0052	0·0052
R	*S*	0	*C*	0·48	0·47	−0·0043	0·0093	0·0070	0·0077
W	*N*	0	*C*	0·69	0·71	−0·011	0·0023	0·0044	0·0042
R	*N*	0	*C*	0·65	0·62	−0·0013	0·012	0·0048	0·0055
W	*S*	1	*C*	0·45	0·49	−0·012	0·0016	0·0050	0·0053
W	*N*	0	X	0·69	0·66	−0·0098	0·0038	0·0037	0·0043
Observed rates versus predicted				—	0·87	—	−0·014	—	0·0015

*Observed rates from field observations (Fig. 4A). Predicted rates from assumption of equilibrium during translation (Fig. 4B). Simulations assume 50% initial saturation, $V_0'(80) = 1000$ cm/sec, and a grain size of 0·25 mm; **C, convergence term in equation 1 is retained; X, convergence effects in equation 1 are omitted; †285 data points from stoss-side used in calculation of results; ‡W, assumed transport following wind streamlines; R, assumed transport following ripple train; §N, direct slope effects upon transport discounted (equations 7–9); S, slope effects on transport given by equation 14.

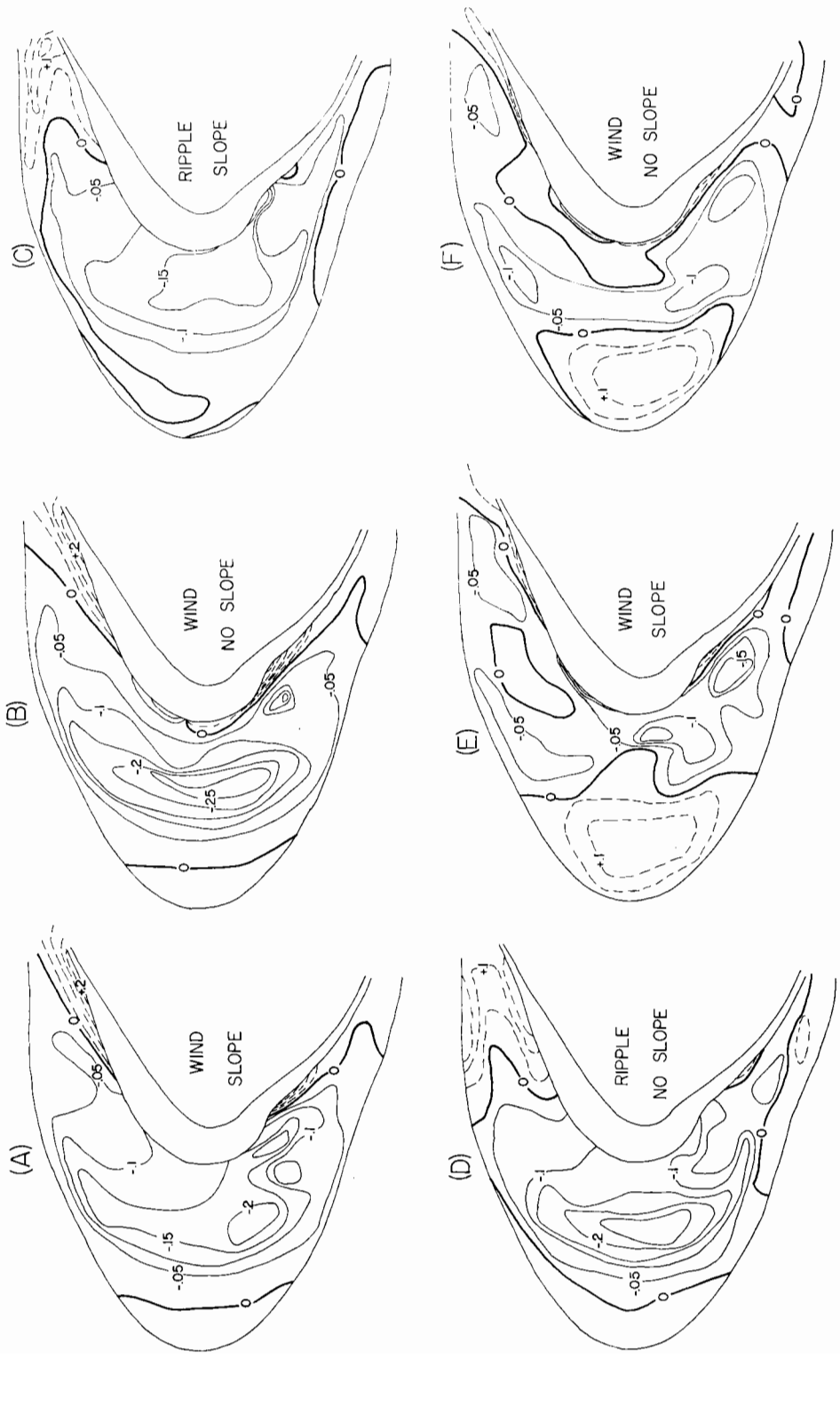

Fig. 10. Simulated erosion and deposition rates (scaled). A–D, simulations for nominal conditions except as indicated: Wind, transport following wind streamlines; ripple, transport along ripple streamlines; slope, slope effects upon transport included; no slope, slope effects discounted; E and F, differences between simulated erosion rates and rates predicted by assumption of equilibrium

through the origin with slope $\delta x/\delta t$ (equation 3). The resulting plots for most simulations appear to be linear, but with considerable scatter, partially due to data errors and partly due to the failure of the assumptions, particularly that of equilibrium with a unidirectional wind (Fig. 11, A–C). The shape of the plots is insensitive to variation in grain size, in velocity, to the transport law assumed, and to inclusion or exclusion of slope effects and convergence. However, the plots are quite sensitive to the assumed transport direction and to the amount of assumed delay. The simulated results following the wind provide a closer approach to theoretical equilibrium than do the ripple train simulations (Fig. 11A and B). For delays greater than about two cells (6 m, prototype scale) the points no longer are consistent with a line passing through the origin (Fig. 11C). This is due to a decrease in the difference in discharge between the high central portions of the brink and the lower wings.

Interpretation

Comparison of the observed, predicted, and simulated patterns of erosion and deposition (compare Figs 4 and 10) reveal that the major discrepancy for assumed transport following both wind and ripple paths is a large underestimate of erosion rates on the stoss side near the toe. In addition, the ripple path simulations indicate a zone of overly-strong deposition along the wingtips of the dune, due to strong flow convergence. The remaining discrepancies are smaller and generally not symmetrically distributed on the two sides of the dune, and may have arisen due to slight differences between the geometry of the prototype and model dune (and its effects upon the near-surface windflow), to local errors in mapping of velocities, or to the effects of non-unidirectional winds. The area of major underestimation of erosion rates near the central upwind edge is possibly due to several factors: (1) differences in dune shape between the model and prototype might have produced unrepresentatively low shear stresses in the discrepant area; (2) flow divergence in the area of question may have been underestimated, which would reduce simulated erosion rates; (3) the change from desert floor to loose sand just upwind from the zone in question may be associated with a change in saltation mechanics which would lead to local scour; (4) when the wind is not unidirectional, but fluctuates (for example, the 30 degree range observed in the field), the hump of the dune along the central line of symmetry will be more strongly eroded than in the case of a unidirectional wind due to greater relative shear stresses on the centreline for skewed oncoming winds (the centreline becomes the crestline for sufficiently skewed winds).

The first three of these potential explanations share a common problem; were the large area of erosional deficit on the central stoss-side eliminated by adding additional sand into transport, the required velocities would be much higher than observed, and the quantity of sand in transport would be greater than would be allowed for brinkline equilibrium. These problems can be quantitatively illustrated by running the simulation model backwards, that is, by assuming that the theoretical erosion rates actually occur and to calculate the necessary distribution of velocity and sand discharge. Such an approach was taken for several combinations of assumed transport law, presence or absence of direct slope effects, wind versus ripple transport paths, and for various wind velocities and grain sizes. Because of the difficulty of unravelling the effects of lags between shear stress and sand transport, all simulations were conducted at zero delay. The resulting hypothetical velocity distributions (Fig. 12) are not

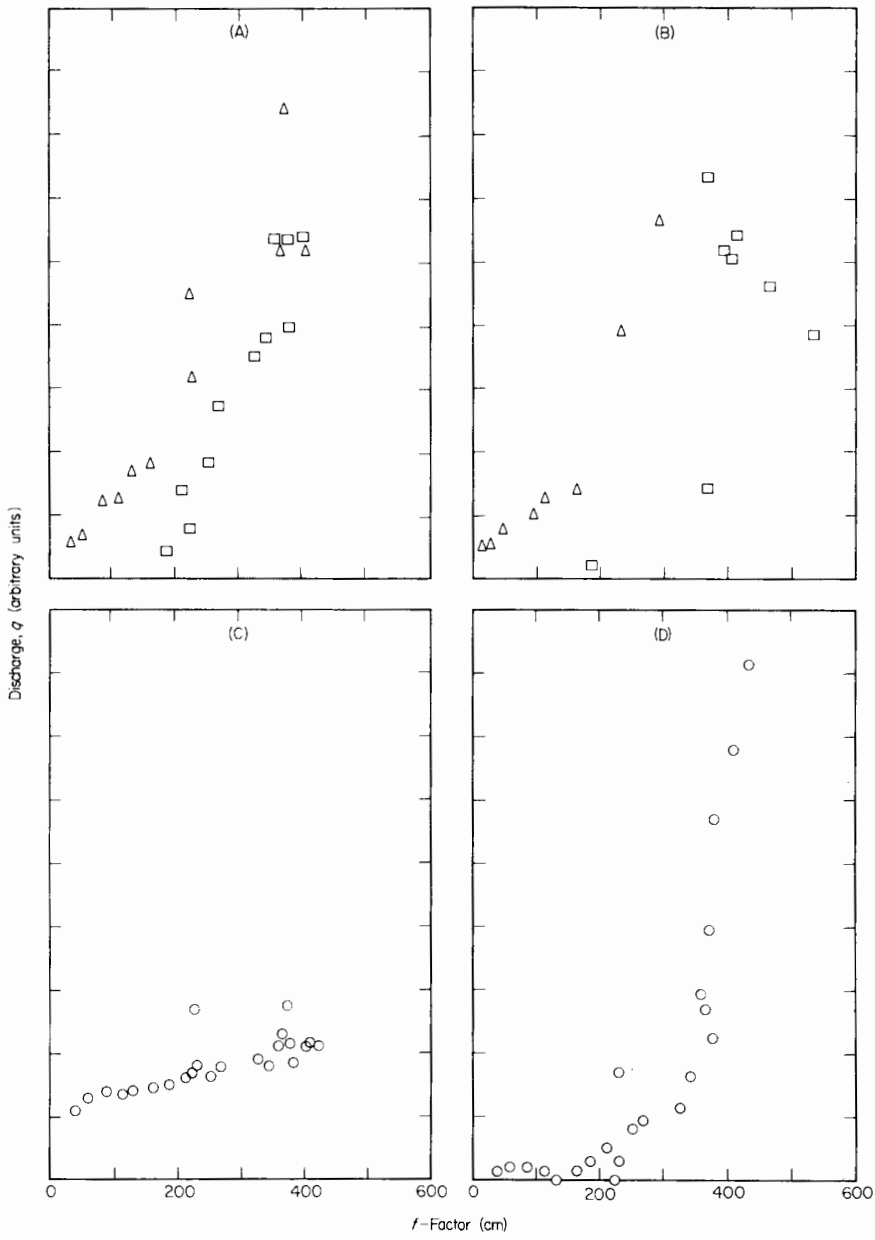

Fig. 11. Relationship between discharge and brink factor, f, for streamline cells terminating on the brinkline. Simulations for nominal conditions except as follows: A, transport following wind streamlines; B, transport following ripple streamlines; C, transport following wind streamlines, average delay of ten cells, saturation of 50%; D, discharge predicted from assumption of equilibrium, transport following wind streamlines; (Squares: left-wing streamline lanes; Triangles: right-wing lanes; Circles: undifferentiated).

markedly different from either field or laboratory measurements of near-surface velocities (Fig. 5) except along the centre of symmetry of the dune, where very high velocities would be required. Relative to both field and laboratory measurements, the required velocities are so much higher than the observed speeds that explanations (1) and (2), above, are clearly inadequate. The third explanation is also rendered questionable by the large quantity of sand that would of necessity be carried over the central portions of the brink if the dune were in strict equilibrium with unidirectional winds (the required discharge follows directly from along-streamline book-keeping of changes in transport rate required by equation (1)). A plot of the required sandflow versus the f-factor for brinkline equilibrium illustrates this (Fig. 11D); the striking upturn of the curve at higher values of q and f (along the central portions of the brink) indicates that equilibrium of the stoss side with unidirectional wind is inconsistent with brinkline equilibrium.

Therefore the prototype barchan appears to be shaped by winds from a range of directions. The observed 30 degree variation in the direction of sand-transporting winds, the asymmetry of the dune, and the non-symmetrical discrepancies between simulated and theoretical distributions of erosion rates support this conclusion. Minor variations in the direction of the oncoming wind can cause large changes in near-surface velocities. As discussed above, those winds arriving at an angle to the direction of symmetry will exert greater shear on the central stoss side relative to a unidirectional wind. The extra sand eroded from the central stoss side would be carried to portions of the brink along the downwind side of the centre, reducing the relative amount of sand flowing over the central brink as compared to that arriving to either side. This redistribution of sand would tend to linearize the relationship shown in Fig. 11D.

Accordingly, a barchan dune shaped by a completely unidirectional wind must have a form somewhat different from one shaped by a more varied wind. In particular, the central axis of the stoss side would have to project further upwind, approaching more closely to a canoe shape. The narrow 'bow' would increase both the shear and divergence on the central stoss, eliminating the zone of underprediction. The average shear on the lower portions of the two wings would be reduced, compensating for the zones of excess erosion simulated on the wings (Fig. 10).

Despite the systematic discrepancies between simulated and theoretical (or empirical) erosion and deposition rates due to variations in direction of the oncoming wind, the model sufficiently reproduces the predicted rates that the assumptions of the model appear to be substantially correct. In particular, the following conclusions are suggested. (1) The prototype dune was near equilibrium with a nearly unidirectional wind. (2) Bagnold-type sand transport equations adequately describe transport over dunes. Simulations neglecting the direct effect of slope on transport rates (equation 14) are slightly better than those that include the effect. (3) Variations in shear over the dune are more important than convergence and divergence in determining the equilibrium of the dune. (4) A delay between downwind changes in shear stress and the resulting rate of sand transport is not needed in order to account for the equilibrium of the dune, and the predictions of the model are less accurate when long delays are assumed. (5) Measurement of the near-surface velocity distribution over the dune (at a scale height of $z/H = 0{\cdot}13$), when combined with equation 4 gives an accurate measure of the surface shear, except perhaps over sharply curved portions of the stoss side. (6) Very similar patterns of erosion and deposition rates are simulated for

transport along wind streamlines and along the ripple train, except on the wings where convergence is strong in the ripple case. This indicates that the shear distribution is more important in determining erosion and deposition rates than is the direction of transport. However, the brinkline is closer to the equilibrium with wind streamline sandflow than with ripple train flow, suggesting that the bulk of the sand closely follows the wind across the dune.

FACTORS CONTROLLING BARCHAN SIZE AND GEOMETRY

The simulation model illustrates several of the interactions between the sediment flow and airflow responsible for creation and regulation of barchan dunes. The development of dunes requires both an initial instability in the transport of sand over a level desert surface, leading to an accumulation of sand, and feedback mechanisms between the airflow and sand transport which limit the growth of the accumulation to a given size and shape. Bagnold (1941, pp. 167–187) felt that the initial instability might arise due to the greater rebound of grains on a desert surface relative to loose sand, allowing oversaturation of sandflow over the desert floor. Irregularities in the desert floor topography may also encourage deposition. Unfortunately, the simulation model offers little evidence regarding the destabilizing mechanisms.

The feedback mechanisms determining equilibrium are clearer. These interactions are of two types, those that control the shape of the dune, and those that affect the size. The regulating mechanisms controlling the shape are more sensitive than those controlling the size, as suggested by several observations. (1) Slight variations in geometry of the dune relative to the oncoming wind cause major changes in the velocity distribution over the dune, and hence, in the spatial pattern of relative erosion and deposition. The effect upon near-surface velocities of variation in direction of the oncoming wind (Fig. 13) illustrates this effect. (2) When a smaller barchan overtakes a larger, the two often unite as a single large dune similar in shape to the original dunes. (3) Field observations indicate that dune shape responds very rapidly to changes in wind direction, so that reorientation to a reversal of wind direction occurs after a relatively short distance of migration (Smith, 1970). Major changes in dune size, however, occur only after the dune has migrated a considerable distance downwind. (4) In a given dune field the largest barchans may be more than ten times the size of the smallest, but large and small barchans differ very little in shape (Finkel, 1959; Coursin, 1964; Hastenrath, 1967).

Dune shape

The factors controlling dune shape will be considered first, and the equilibrium of the stoss-side will be considered separately from that of the brinkline. This seems justified because the flow over the stoss slope is little affected by the separated flow downwind from the brink.

The barchan is shaped approximately like the chordal section of an ellipsoid of revolution (a 'whaleback') with the downwind portion scooped out. Thus the stoss side geometry can be roughly characterized by two ratios, H/W and W/L, where H is the crest height, W is the wing-to-wing width transverse to the flow, and L is the distance from the tip of the windward edge to the crest. If H/W were larger than on the

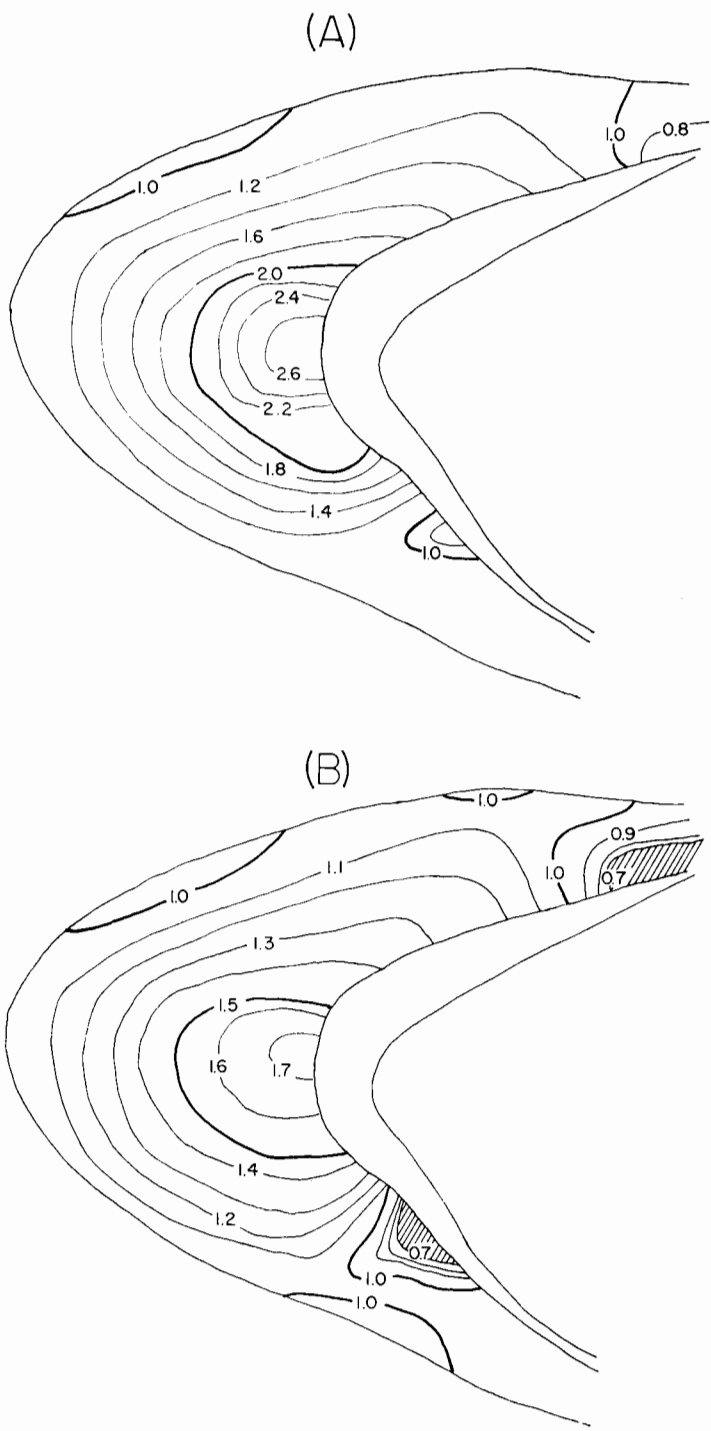

Fig. 12. Velocities ($v(80)/v_0(80)$) necessary to produce predicted erosion rates for unidirectional wind. A, simulation following wind streamlines with slope effects retained; B, same except slope effects discounted. Hatched areas indicate regions where amount of sediment in transport is insufficient to match predicted erosion rates.

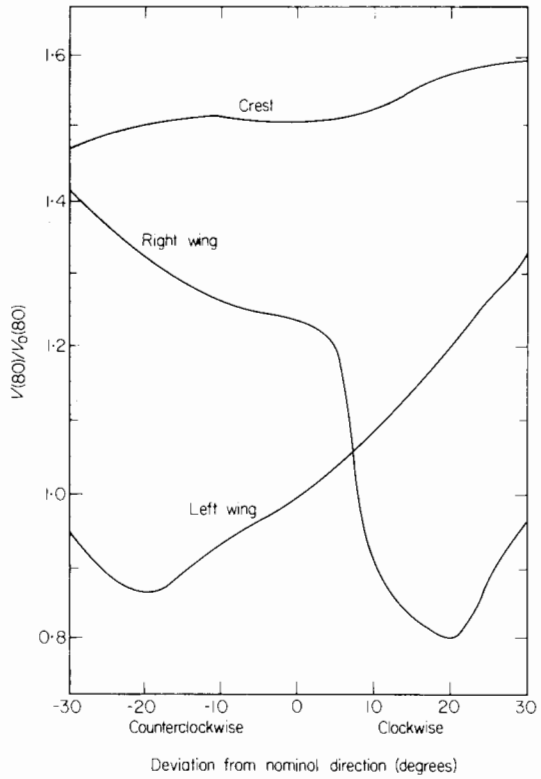

Fig. 13. O. Effect of variation in direction of oncoming wind upon velocities ($v(80)/v_0(80)$) measured at three brinkline locations on the model dune (see Fig. 5).

prototype barchan (W/L constant), the shear stress on the crest would be increased relative to the basal portion of the dune, the streamlines near the toe would be more divergent, and the steeper gradients would cause a greater downgradient component to the sediment flow, reducing sand delivery to the crest. All these factors cause a more rapid crestal erosion, tending to return the dune to equilibrium. Similarly, if the W/L ratio were increased from its value on the present dune (H/W constant), the shear stress on the central stoss near the toe would be reduced relative to the wings, whereas the wings would be more exposed. Sediment transport over the central toe would lag relative to the wings and crest (due to both reduced shear and steeper upslope gradient), tending to restore equilibrium (although a greater flow divergence would partially counteract the sheltering of the central leading edge). The overall streamlined shape and the gradual tapering of the height from the centre of the dune to the leading edge is due to the very rapid erosion that would occur to any mass of sand that projected sharply into the wind.

The effects of variations of grain size and velocity upon dune shape are indicated by the relative rates of erosion on the basal wings (w areas, Fig. 2A), the central leading edge (l area), and on the crest (Area h). The average rates of erosion, $\bar{E}_w$, $\bar{E}_h$, and $\bar{E}_l$, were calculated for each simulation for the streamline cells within the respective areas, pooling the w_1 and w_2 areas, so that variations in the ratios $\bar{E}_w/\bar{E}_h$ and $\bar{E}_l/\bar{E}_w$ are indices of predicted variations of H/W and W/L, respectively, that would

accompany change in grain size and velocity. These ratios suggest that either an increase in wind speed or a decrease in grain size should cause a moderate increase in H/W and a rapid increase in W/L, that is, the dune would be steeper and more blunt.

Increase in the assumed delay between changes in shear stress and sand transport rate tends to increase H/W and marginally to decrease W/L.

The equilibrium of the brinkline is more complex due to the upwind influence of the separated flow, leading to interaction between changes in brinkline shape and the geometry of the stoss side. The brinkline can adjust to lateral differences in sand supply by change in planfrom curvature of the brinkline, which affects H_e, by change in orientation relative to the oncoming wind, which affects the angular relationships on the right-hand side of equation 3, and by change in shear stress as the position of brink varies relative to the dune tip.

Changes in curvature are the most important regulating mechanism near the crest of the barchan. Near-surface velocities drop off very slowly away from the crest (Fig. 5). Therefore, if the brinkline were, for example, initially straight and perpendicular to the sandflow, the central part would migrate less rapidly than the adjacent lower brinkline which receives nearly the same sand supply but has a lower slip face. The crestal lag would create a concave curvature of the slip face, reducing the area of deposition and speeding up the brink movement. Such a feedback mechanism creates a stable, sharply-curved crestal brinkline.

The orientation of the brinkline on the wings is due to a more complex interaction of the terms in equation 3. The brinkline here is nearly linear, so that curvature is not a factor. These interactions can be illustrated by disturbing the natural brinkline by an incremental forward displacement of the wings relative to the central brink. Comparing points of equal elevation on the displaced and original brinkline the inward curvature of streamlines near the crest implies a decrease in ζ and an increase of ω. Thus the angular terms in equation 3 imply, other factors being equal, a slight increase in the rate of downwind translation of the brinkline, a destabilizing influence. However, this is overbalanced by the decrease in transport rate that occurs due to the greater sheltering of the advanced brinkline from the wind (on the barchan wings, velocity decreases along the contours as the crest is approached, see Fig. 5). Thus a displacement of the brinkline on the wings causes a return toward equilibrium.

The position of the brink relative to the upwind edge is likewise a function of the sediment budget. A slip face will not be stable unless an overall divergence of sandflow occurs on the stoss edge to compensate for sand supplied from upwind and for the inward convergence of sand avalanching down the slip face. A balance must also, of course, be maintained between interception of sand from upwind and loss from the dune by streamers from the barchan wing tips (Bagnold, 1941, p. 212; Lettau & Lettau, 1969).

The factors controlling the position of the brink relative to the upwind edge of the dune can be illustrated by first considering the equilibrium of a laterally-infinite two-dimensional dune oriented transverse to the flow. Equations 1 and 2 imply for such a dune at equilibrium that.

$$\frac{1}{\gamma}\frac{q}{h} = \frac{\delta x}{\delta t} = K, \text{ or } \frac{q}{\gamma} = K h + \frac{q_0}{\gamma} \tag{23}$$

where K is constant for the given dune. However, a slip face with its brink at a given height, h, must migrate forward at a rate $K' = q/\gamma h$. Thus a slip face on an infinite two-dimensional transverse dune trapping all sand received from upwind is unstable, for it will always migrate forward faster than the dune as a whole. However, on a barchan the sandflow diverges as its crosses the stoss side, gradually reducing K' downstream so that at some point a brink can exist in equilibrium with the stoss side migration rate. As an example, the case of an idealized stoss slope with flow divergence will be considered. For this example, the streamlines diverge at a constant angle, φ (which must be zero on a two-dimensional dune) over the stoss side which is dripping towards the oncoming wind with a constant gradient (Tan θ). At the upwind edge the transport rate is q_0 and the initial width of the streamline lane is l_0. The brinkline is assumed to be perpendicular to the crest, with no curvature. Under such conditions, equations 1, 2, 3, and 18 indicate that the brink can exist in stable equilibrium with a stoss side of length x, given by:

$$x = \left(\frac{2 q_0 l_0}{\gamma \varphi K \operatorname{Tan} \theta} \right)^{\frac{1}{2}} \tag{24}$$

This regulation of the position of the brink relative to the crest occurs primarily along the dune wings, because the central portions of the brink adjust by change of orientation and curvature (in fact, the flow there may converge slightly, see Fig. 2A).

Equation 24 also explains the forward displacement of the brinkline on the lower dunes within a field of barchans. The smaller dunes have lower values of H/W (Finkel, 1959; Hastenrath, 1967), so that both the average stoss slope, θ, and the flow divergence, φ, are less, requiring the relatively longer stoss side (the migration rate of dunes is approximately inversely proportional to crest height, as is the scale width, l_0, whereas q_0 is presumably uniform).

The adjustment of the dune to variations in the saturation of the oncoming sandflow is less certain, as is the total range of saturation for which barchans are stable. A low saturation implies a greater potential for erosion along the upwind edge, resulting in a steeper dune and increased divergence at the upwind edge, causing a large W/L ratio. Equation 24 suggests that the brink should lie closer to the upwind edge. An open, crescent-moon-shaped dune that is more nearly two-dimensional should result. A whaleback form with a small slip face would probably characterize a barchan with a large saturation.

Dune size

Barchan dunes vary from a few metres in width to several hundred metres. The factors controlling their size may reside either in natural scales of atmospheric turbulence or in the sand transport processes. For example, ripple scale appears to be determined by the average path length of sand in saltation (Ellwood *et al.*, 1975), whereas the size of the largest dunes (draas) may be related to large convection cells with wavelengths on the order of the thickness of the atmospheric boundary layer (Wilson, 1972; Hanna, 1969; Wipperman, 1969). But the factors controlling the scale of the large class of dunes ranging from about 10–500 m in size are less certain. Wilson (1972) feels that their scale is controlled by transport properties, such as grain size,

velocity, and saturation, while Cooke & Warren (1973) suggest natural atmospheric scales. The observations of Wilson (1972, Fig. 2) suggest that dune size increases with grain size. Unfortunately, little other systematic data has been collected. Unlike subaqueous flows, where the depth imposes a natural scale on dunes, atmospheric boundary layer flows do not have as well-defined a natural scale. In the surface layer, a zone about 50–200 m deep in which Coriolis effects are negligible and the shear stress is nearly constant with height (Plate, 1971; Lumley & Panofsky, 1964), the natural scaling factor is the aerodynamic roughness. Most natural dunes are deeply submerged in this layer.

Transport-related scale factors might emerge from two length scales, (1) the distance lag between change of shear stress and response of the saltation load, and (2) upwind roughness length z_0 (or z_{0a}). The simulation model suggests that the first of these factors is unimportant, except that it sets a minimum size for a stable dune (Bagnold, 1956, p. 296). A sand body of the same size as or smaller than the distance lag would not have the variance in transport rates necessary to cause the pattern of erosion and deposition necessary for equilibrium. This minimum size is probably proportional to the average path length of grains in saltation, and hence, like ripple wavelength, the minimum wavelength would increase with larger grain size and stronger wind shear.

Dune scale may also be affected by roughness length, because variations in roughness change the pattern of wind shear on the dune. The possible influence of roughness was illustrated through a heuristic model by Howard *et al.* (1977) which assumes that large and small dunes are geometrically similar. This assumption, when combined with sand transport equations and the numerical simulations of turbulent flow by Taylor & Gent (1974), suggest that dune size would be proportional to the upwind roughness and that the relative dune steepness, H/L, is independent of dune scale. If the upwind roughness is controlled by fixed roughness elements, such as the rock cover on the desert floor or vegetation, then dune size would, if this model is realistic, be larger the greater the upwind roughness. However, no systematic data is available on the correlation between dune size and the upwind roughness.

If the natural roughness elements are small, and the sandflow is near saturation, the roughness will be controlled by the saltation process, as indicated by equation 6. This equation, together with equation 11, relating U_t to grain size, indicate that the upwind roughness increases as u_{*0} increases, but decreases as grain size increases (for a constant upwind shear velocity). Thus, if dune size is proportional to the saltation roughness, grain size and dune scale would be inversely correlated. This is opposite to the direct proportionality observed by Wilson (1971). However, the dominant shear stress for dune formation increases with grain size, due to the greater threshold velocity. Depending upon the natural variation with grain size of the ratio of dominant shear stress to threshold shear, the saltation roughness (and the dune size) might either remain constant or increase as grain size becomes larger.

The elapsed time since initiation of the dune may be an important scale factor. In a field of barchans new dunes appear to originate as small whaleback dunes in the streamers from larger barchans or from the breakup of larger dunes. Due to the inverse relationship between dune height and migration rate (Bagnold, 1941, p. 214; Hastenrath, 1967; Coursin, 1964), large barchans are often overtaken by smaller and their merger frequently creates a single dune of larger size. The merger process encourages development of equal-sized dunes which do not collide because of equal rates of

movement (Rim, 1958). Thus dune scale may be time dependent. Whether natural atmospheric, roughness, or transport scales impose an upper as well as lower limit to barchan size is at present uncertain.

CONCLUSIONS — RESEARCH NEEDS

If the interactions between sand transport, dune form and fluid flow could be completely modelled, the limits of stability of the dune and the factors controlling the form and size of the dune could be readily determined. Ideally, such a model should first predict the air flow over any three-dimensional sand deposit protruding from a level desert surface, including particularly the streamline pattern near the surface and the shear stress distribution. Then, using appropriate bedload transport equations, the obstacle would be modified by erosion and deposition in a simulation model, proceeding by steps to an equilibrium form (if, indeed, one is established). Thereupon the effects of variation in wind velocity, in quantity of supplied sand, in roughness length, in grain size, and in constancy of wind direction could be investigated. Unfortunately, theoretical modelling of fluid flow around three-dimensional objects with arbitrary boundary conditions, while conceptually feasible, requires extensive computations. The authors are presently attempting to develop an efficient computer simulation model.

A parallel need exists for comprehensive field measurements of sand flow (quantity, grain size, and vertical distribution) and the associated velocity profiles at many points on and upwind from natural dunes in order to refine the model presented here.

ACKNOWLEDGMENTS

Lunar and Planetary Programs, supported by the National Aeronautics and Space Administration, Contract NGR-47-005-172. The manuscript was substantially improved as a result of comments by George Hornberger.

REFERENCES

ALLEN, J.R.L. (1968) *Current Ripples, Their Relation to Patterns of Water and Sediment Motion.* North Holland, Amsterdam.

BAGNOLD, R.A. (1941) *The Physics of Blown Sand and Desert Dunes.* Methuen, London.

BAGNOLD, R.A. (1956) Flow of cohesionless grains in fluids. *Trans. R. Soc. Lond.* **249,** 235–297.

BAGNOLD, R.A. (1973) The nature of saltation and of 'bed-load' transport in water. *Proc. R. Soc.* **332A,** 463–504.

CHEPIL, W.S. & WOODRUFF, N.P. (1963) The physics of wind erosion and its control. *Adv. Agron.* **15,** 211–302.

COOKE, R.V. & WARREN, A. (1973) *Geomorphology in Deserts.* Part 4. University of California Press, Berkeley.

COURSIN, A. (1964) Observations et expériences faites en avril et mai 1956 sur les barkhanes du Souehel el Abiodh (région est de Port-Étienne). *Bull. Inst. fr. Afr. noire,* **26A,** 989–1022.

ELLWOOD, J.M., EVANS, P.D. & WILSON, I.G. (1975) Small scale eolian bedforms. *J. sedim Petrol.* **45,** 554–561.

FINKEL, H.J. (1959) The barchans of southern Peru. *J. Geol.* **67,** 614–647.

GAD-EL-HAK, M., PIERCE, D., HOWARD, A. & MORTON, J.B. (1976) Interactions of unidirectional winds with an isolated barchan sand dune. Technical Report, University of Virginia, Charlottesville.

HANNA, S.R. (1969) The formation of longitudinal sand dunes by large helical eddies in the atmosphere. *J. appl. Met.* **8,** 874–883.

HASTENRATH, S.L. (1967) The barchans of the Arequipa region, southern Peru. *Z. Geomorph.* **11,** 300–311.

HOWARD, A.D. (1977) Effect of slope on the threshold of motion and its application to orientation of wind ripples. *Bull. Geol. Soc. Am.* **88,** 853–856.

HOWARD, A.D., MORTON, J.B., GAD-EL-HAK, M. & PIERCE, D.B. (1977) Simulation model of erosion and deposition on a barchan dune. *NASA Contractor Rpt.* CR-2838.

IVERSON, J.D., POLLACK, J.B., GREELEY, R. & WHITE, B.R. (1976) Saltation threshold on Mars: the effect of interparticle force, surface roughness, and low atmospheric density. *Icarus,* **29,** 381–393.

KENNEDY, J.F. (1969) The formation of sediment ripples, dunes, and antidunes. *Ann. Rev. Fluid Mech.* **1,** 147–169.

LETTAU, K. & LETTAU, H. (1969) Bulk transport of sand by the barchans of the Pampa de Lay Joya in southern Peru. *Z. Geomorph.* **13,** 182–195.

LETTAU, K. & LETTAU, H. (in press) Experimental and micrometeorological field studies of dune migration. In: *Exploring the World's Driest Climate* (Ed. by K. Lettau and H. Lettau). University of Wisconsin Press, Madison.

LONG, J.T. & SHARP, R.P. (1964) Barchan-dune movement in the Imperial Valley, California. *Bull. Geol. Soc. Am.* **75,** 149–156.

LUMLEY, J.L. & PANOFSKY, H.A. (1964) *The Structure of Atmospheric Turbulence.* John Wiley, New York.

MCKEE, E.D. (1966) Structures of dunes at White Sands National Monument, New Mexico (and a comparison with structures of dunes from other selected areas). *Sedimentology,* **7,** 1–69.

MELTON, F.A. (1940) A tentative classification of sand dunes: its application to dune history in the southern high plains. *J. Geol.* **48,** 113–174.

PLATE, E.J. (1971) *Aerodynamic Characteristics of Atmospheric Boundary Layers.* A.E.C. Critical Review Series.

RAUDKIVI, A.J. (1966) Bed forms in alluvial channels. *J. Fluid Mech.* **26,** 507–514.

REYNOLDS, A.J. (1965) Waves on the erodible bed of an open channel. *J. Fluid Mech.* **22,** 113–133.

RIM, M. (1958) Simulation, by dynamical model, of sand tract morphologies occurring in Israel. *Bull. Res. Coun. Israel.* **7G,** 123–136.

SMITH, R.S.U. (1970) Migration and wind regime of small barchan dunes within the Algodones dune chain, Imperial County, California, Unpublished dissertation, University of Arizona.

TAYLOR, P.A. & GENT, P.R. (1974) A model of atmospheric boundary-layer flow above an isolated two-dimensional 'hill'; an example of flow above 'gentle topography'. *Boundary-Layer Met.* **7,** 349–362.

WILLIAMS, G. (1964) Some aspects of the eolian saltation load. *Sedimentology,* **3,** 257–287.

WILSON, I.G. (1971) Desert sandflow basins and a model for the development of ergs. *Geog. J.* **137,** 180–197.

WILSON, I.G. (1972) Aeolian bedforms—their development and origins. *Sedimentology,* **19,** 173–210.

WIPPERMAN, F. (1969) The orientation of vortices due to instability of the Ekman-boundary. *Beitr. Phys. Atmos.* **42,** 225–244.

ZINGG, A.W. (1953) Wind-tunnel studies of the movement of sedimentary material. *Proc. 5th Hydraul. Conf.,* Iowa State Univ. 111–125.

(*Manuscript received* 14 *March* 1977; *revision received* 15 *September* 1977)